# A facile, green fabrication of aqueous nanofluids containing hydrophilic functionalized carbon nanotubes toward improving heat transfer in a closed horizontal flow passage

Akram, Naveed; Hosseini, Maryam; Sadri, Rad; Kazi, S.N.; Kasaeian, Alibakhsh; Yarmand, H.; Hooman, Kamel; Ahmad, Roslina

**DOI**
10.1016/j.powtec.2022.117451

**Publication date**
2022

**Document Version**
Final published version

**Published in**
Powder Technology

**Citation (APA)**
Akram, N., Hosseini, M., Sadri, R., Kazi, S. N., Kasaeian, A., Yarmand, H., Hooman, K., & Ahmad, R. (2022). A facile, green fabrication of aqueous nanofluids containing hydrophilic functionalized carbon nanotubes toward improving heat transfer in a closed horizontal flow passage. *Powder Technology*, *404*, Article 117451. https://doi.org/10.1016/j.powtec.2022.117451

Powder Technology 404 (2022) 117451

Contents lists available at ScienceDirect

Powder Technology

journal homepage: www.elsevier.com/locate/powtec

# A facile, green fabrication of aqueous nanofluids containing hydrophilic functionalized carbon nanotubes toward improving heat transfer in a closed horizontal flow passage

Naveed Akram [a,b], Maryam Hosseini [c], Rad Sadri [d,*], S.N. Kazi [a,*], Alibakhsh Kasaeian [d], Hooman Yarmand [e], Kamel Hooman [f], Roslina Ahmad [g]

[a] Department of Mechanical Engineering, Faculty of Engineering, University of Malaya, Kuala Lumpur 50603, Malaysia
[b] Department of Mechanical Engineering, Mirpur University of Science and Technology (MUST), Mirpur 10250, AJK, Pakistan
[c] School of Chemical Engineering, The University of New South Wales, Sydney, NSW 2052, Australia
[d] Faculty of New Sciences and Technologies, University of Tehran, Tehran, Iran
[e] Department of Sustainable Design Engineering, Faculty of Industrial Design Engineering, Delft University of Technology, 2628 CE Delft, the Netherlands
[f] School of Mechanical and Mining Engineering, The University of Queensland, QLD 4072, Australia
[g] Centre of Advanced Materials, Department of Mechanical Engineering, Faculty of Engineering, Universiti Malaya, 50603 Kuala Lumpur, Malaysia

ARTICLE INFO

*Article history:*
Received 22 November 2021
Received in revised form 16 April 2022
Accepted 26 April 2022
Available online 29 April 2022

*Keywords:*
Nanofluid
Thermo-physical properties
Thermal conductivity
Convective heat transfer
Multiwalled carbon nanotubes
Environmentally friendly

ABSTRACT

In the present research, the synthesis of highly stable multiwalled carbon nanotubes in aqueous media is developed using a one-pot, covalent and green functionalization technique to improve the heat transfer and hydrodynamic behavior of a horizontal stainless-steel tube subjected to a uniform heat flow at its outer surface. Instead of using corrosive inorganic acids, the free radical grafting of gallic acids is used in this procedure. In this work, GA-functionalized multiwalled carbon nanotubes water-based colloidal suspensions (nanofluids) were prepared at three different weight concentrations. Various characterization techniques comprising Fourier transform infrared spectroscopy, Raman spectroscopy, High resolution transmission Electron Microscopy, and zeta-potential measurements were performed and confirmed the success of MWCNT functionalization. The thermophysical properties were evaluated experimentally and validated using empirical correlations available in the literature. To prove the colloidal suspension stability, ultraviolet-visible spectroscopy was used, and the results showed that nanofluid was stable for almost 60 days. When the GAMWCNT concentration was increased, there was a significant improvement in the thermal conductivity. Moreover, the nanofluids' dynamic viscosity experienced a slight increment up to 7.30% when the GAMWCNTs were loaded relative to distilled water. Following the confirmation of the experimental setup's analytical correlations, tests for the colloidal GAMWCNT suspension flowing through a heated horizontal tube were carried out in a fully developed turbulent state. A significant enhancement in the convective heat transfer coefficient was obtained, with only minor growth in the relative pumping power by 33.05 and 1.19%, respectively. More importantly, the reported positive performance index indicator for all the Reynolds numbers of ranges shows the possibility of using the synthesized GAMWCNT aqueous suspensions as an alternative working fluid in heat transfer systems.



## 1. Introduction

Convective heat transfer plays a crucial role in various thermal systems (e.g., heating and cooling devices and solar collectors). However, the applicability and performance of heat transfer systems is restricted by the low heat conductivity of traditional refrigerants (e.g., ethylene glycol, oil, and water) [1,2]. Therefore, scientists and researchers are actively seeking how alternative coolants can be generated with improved thermal conductivity to boost the performance of thermal applications [3,4]. In this respect, experimental and computational investigations have been conducted on thermal systems, where nanofluids are employed as operating fluids to analyze the heat transfer and hydrodynamic characteristics. Nanofluids are mainly nanoparticles blend immersed in the base fluid (e.g., water). Nanofluids are effectively used for convective heat transfer applications due to the higher thermal conductivity relative to conventional working fluids [5–8].

* Corresponding authors.
*E-mail addresses:* Rod.sadri@gmail.com (R. Sadri), Salimnewaz@um.edu.my (S.N. Kazi).

https://doi.org/10.1016/j.powtec.2022.117451
0032-5910/

**Nomenclature**

| | |
|---|---|
| A | internal surface area of the tube ($m^2$) |
| NIST | National Institute of Standards and Technology (NIST) |
| $C_p$ | specific heat capacity (J/kg K) |
| CNT | carbon nanotube |
| MWCNT | multi walled carbon nanotube |
| GAMWCNT | Gallic Acid-treated MWCNT |
| D | tube diameter (m) |
| TEM | transmission Electron Microscopy |
| GA | Gallic Acid |
| *wt%* | weight percentage/mass fraction |
| $\dot{w}$ | pumping power |
| $k$ | thermal conductivity, W/m.K |
| L | tube length (m) |
| $\dot{m}$ | mass flow rate (kg/s) |
| UV-VIS | ultraviolet-visible spectroscopy |
| *Pr* | Prandtl number |
| Q | input power (Watts) |
| $\dot{q}$ | heat flux ($W/m^2$) |
| *Nu* | Nusselt number |
| $f$ | friction factor |
| h | convective heat transfer coefficient |
| *Re* | Reynolds number |
| V | voltage ($v$) |
| T | temperature, °C |
| I | current (A) |
| $v$ | velocity, m/s |
| FTIR | Fourier transform infrared spectroscopy |
| $T_w$ | wall temperature (K) |
| $T_i$ | inlet fluid temperature (K) |
| $T_o$ | outlet fluid temperature (K) |
| $T_b$ | bulk temperature (K) |

*Greek symbols*

| | |
|---|---|
| $\varepsilon$ | performance Index |
| $\rho$ | density of the fluid ($kg/m^3$) |
| Δp | pressure drop (Pa) |
| μ | dynamic viscosity (mPa.s) |

*Subscripts*

| | |
|---|---|
| bf | base fluid |
| nf | nanofluid |
| NPs | nanoparticles |
| b | bulk |
| i | inlet |
| m | mass |
| o | outlet |
| t | thermocouple |
| w | wall |
| avg | average |

So far Specific nanoparticles have been employed to produce nanofluids with high thermal conductivity, for example carbon nanomaterials like carbon nanotubes (CNTs) [3,9], and graphene [10–14], in addition to metal oxides like copper oxide (CuO) [15,16], Iron Oxide ($Fe_2O_3$) [17], aluminum oxide ($Al_2O_3$) [4,18–20], and silicone dioxide ($SiO_2$) [17].

Nanofluids have been utilized in various thermal applications, comprising the microchannel, solar collectors [21,22], and heat recovery systems. During various numerical and experimental studies in different types of pipes, the influence of employing nanofluids as alternatives to traditional working fluids has been observed as the modes and structures of heat exchanger pipes vary according to their applications [23,24]. Theoretical and experimental studies of nanofluids have been conducted in different flow regimes to achieve high heat transfer performance and low-pressure reduction in square and rectangular conducts. [25–27]. All of the experiments demonstrated a substantial improvement in heat transfer when nanofluids were used as the working fluid, where the pressure drop also increased. Despite the variety of pipe shapes and designs, circular tubes are still considered the most common type of tube in engineering applications.

Fotukian and Esfahany experimentally investigated the convective heat transfer and pressure drop for a nanofluid with 0.24 vol% of CuO (where water was used as the base fluid) passing through a circular pipe [28]. The convective heat transfer improved by 25%, whereas the pressure drop decreased by 20%. Sajadi and Kazemi reported 25% improvement in convective heat transfer in a circular tube under turbulent flow regime when 0.24 vol% of $TiO_2$ nanoparticles were loaded into the base fluid [29]. The highest pressure drop (25%) was attained at $Re = 5000$ for the nanofluid containing 0.25 vol% of nanoparticles. They proposed a Nusselt number ($Nu$) correlation for the single-phase fluid. Esfe et al. conducted an experimental study on the effect of MgO/water nanofluid on the heat transfer coefficient in a circular pipe [30]. They found 35.93% improvement at a nanoparticle concentration of 0.1 vol% and $Re = 7331$. Li et al. reported a 13.62% improvement in thermal conductivity of ZnO/EG-W nanofluid at a nanoparticle concentration of 5 wt% [31]. They demonstrated that the convective heat transfer coefficient of the prepared nanofluid increased as the *Re* increased, and they reported 30% enhancement at a nanoparticle concentration of 2.5 wt%. Devi et al. conducted a numerical and experimental investigation on the effect of $Al_2O_3$/water and CuO/water nanofluids as coolants in a circular tube [32]. They considered a nanofluid volume concentration of 1% and 3% in the laminar regime. The *Nu* of both nanofluids improved substantially; however, the $Al_2O_3$/water nanofluid showed better heat transfer coefficient values than the CuO/water nanofluid.

Among nanoparticles, carbon nanostructures have remarkable physical, chemical, and mechanical properties, along with high thermal conductivity, rendering these materials a promising candidate for heat transfer applications. Carbon nanotubes (CNTs), a family of carbon-based materials is suitable for diverse applications, comprising heat transfer coolant and supercapacitor owing to their high durability, low density, good reliability, and excellent electrical, thermal, and mechanical characteristics. Nevertheless, the main obstacle in their usage is their low solubility. CNTs are readily entangled as a result of strong intermolecular π-π interactions and appear to aggregate in polar solvents such as ethylene glycol and water [33–35]. In industrial applications, this obstructs the process capability of CNTs. Hence, numerous procedures have been employing to improve the stability and solubility of carbon-based materials in aqueous and organic media, such as covalent and noncovalent functionalization of these materials. The covalent functionalization of carbon-based materials has been used to produce stable nanofluids and has attracted considerable attention among researchers and scientists. In this method, the hydrophilic functional groups for instance amine, carboxyl acids, or esters are attached onto the surface of the carbon-based materials employing either one of the following reaction methods: amination, oxidation, esterification, nucleophilic addition, or free radical grafting of CNTs with strong acids [6,36]. Despite these chemical methods are commonly reliable in synthesizing functionalized CNTs, these routes are not environmentally friendly because the reagents used are toxic and environmentally harmful. Even more importantly, some of these chemical paths may cause lattice defects, which weaken the inherent CNT features. [33].

Recently, a new pathway of covalent functionalization of carbon nanomaterial based on employing natural materials such as herbs was introduced by our research group. In this work, clove buds [37] have shown outstanding properties in improving the stability and solubility

of CNTs in an aqueous medium. It has been noticed an improvement in the thermophysical characteristics of the base fluid (i.e. Water) after full dispersion of the nanoparticles. The heat transfer and hydrodynamic behavior for the clove-treated MWCNT/water nanofluids (C-MWCNT/water) were investigated experimentally and numerically using an annular heat exchanger subjected to a uniform heat flux. The findings are promising as the C-MWCNT/water nanofluids were considerably more thermally conductive, while the density and viscosity of the nanofluids showed only a minor increase. The Nusselt number and convective heat transfer improved markedly for the C-MWCNT/water, while the increment in the friction factor was marginal.

Gallic acid (GA) is a polyphenol antioxidant extracts from various types of vegetables such as berries, green tea and grapes. [38] GA is widely utilized in various industries comprising food and pharmaceutical. Owing to its composition (phenol) and green characteristics, GA has the potential to be used as a suitable candidate for functionalization of MWCNTs in order to make the surface of MWCNTs hydrophilic and improve their solubility and stability in aqueous media.

In this research, a green, non-corrosive and facile technique is developed for covalent functionalization of MWCNTs using GA via free radical grafting of GA onto the surface of MWCNTs. This technique is particularly advantageous due to the anti-oxidation, non-corrosive and non-toxic properties of GA. To verify the success of the covalent functionalization procedure, both pristine and functionalized MWCNTs are characterized by Fourier transform infrared spectroscopy, Raman spectroscopy, ultraviolet/visible absorption spectroscopy, transmission electron microscopy, and zeta potential measurements to verify the practical application of the functionalization and stability of GAMWCNTs. Next, highly stable GA-treated MWCNTs aqueous suspensions are prepared in different weight concentrations. Following this, the rheological and thermo-physical characteristics of the GA-treated MWCNTs are measured as a function of temperature. Afterward, the effectiveness of the prepared nanofluids in improving the convective heat transfer and hydrodynamic behavior in a closed horizontal circular flow passage subjected to a uniform heat flux is investigated experimentally under turbulent flow conditions.

## 2. Materials and methods

### 2.1. Materials

Pristine MWCNTs (diameter: <8 nm, purity: >95%, specific surface area: >500 $m^2/g$) were sourced from Nanostructured & Amorphous Materials Inc., USA. The remaining chemical reagents were of analytical grade, namely, G.A. (3,4,5-trihydroxy benzoic acid) and hydrogen peroxide ($H_2O_2$, 30%) which were supplied by Sigma-Aldrich.

### 2.2. Synthesis of GAMWCNT/water nanofluids

To functionalize the MWCNTs, 5 g pure MWCNT and 15 g GA were poured into a beaker containing 1000 ml distilled water (DI water) and stirred for 15 min at 80 °C on a hot-plate magnetic stirrer to obtain a homogenous black suspension. In the next step, 25 mL of concentrated hydrogen peroxide (30%) as an initiator was gradually added under vigorous stirring. The blend was ultrasonicated via a sonicator probe for 20 min. After sonication, the mixture was heated at 80 °C under reflux on the hot-plate magnetic stirrer for 14 h. Afterward, the resulted black suspensions containing functionalized MWCNTs were centrifuged and washed several times with abundant DI water until a neutral pH was reached. The GA-functionalized MWCNTs (GAMWCNTs) were dried at 60 °C under vacuum overnight. Introduction of hydrophilic functional groups such as –COOH, –OH in sidewalls, and tips of MWCNTs render them highly dispersible in water for convective heat transfer applications. Fig. 1 represents the procedure of the covalent functionalization of MWCNTs gallic acid. The corresponding homogeneous colloidal suspensions (Nanofluids) were prepared by sonicating 0.025, 0.075, and 0.1 wt% of GAMWCNTs in DI water for 10 min.

Fig. 2 demonstrates the proposed free radical grafting reaction of gallic acid (GA) and MWCNTs in aqueous media. In the first step (initiation step), hydrogen peroxide becomes unstable at high temperatures and decomposes spontaneously into hydroxyl radicals [39]. These hydroxyl radicals attack the GA to create free radicals on the GA molecules, which results in covalent bonding of the activated molecules onto the surface

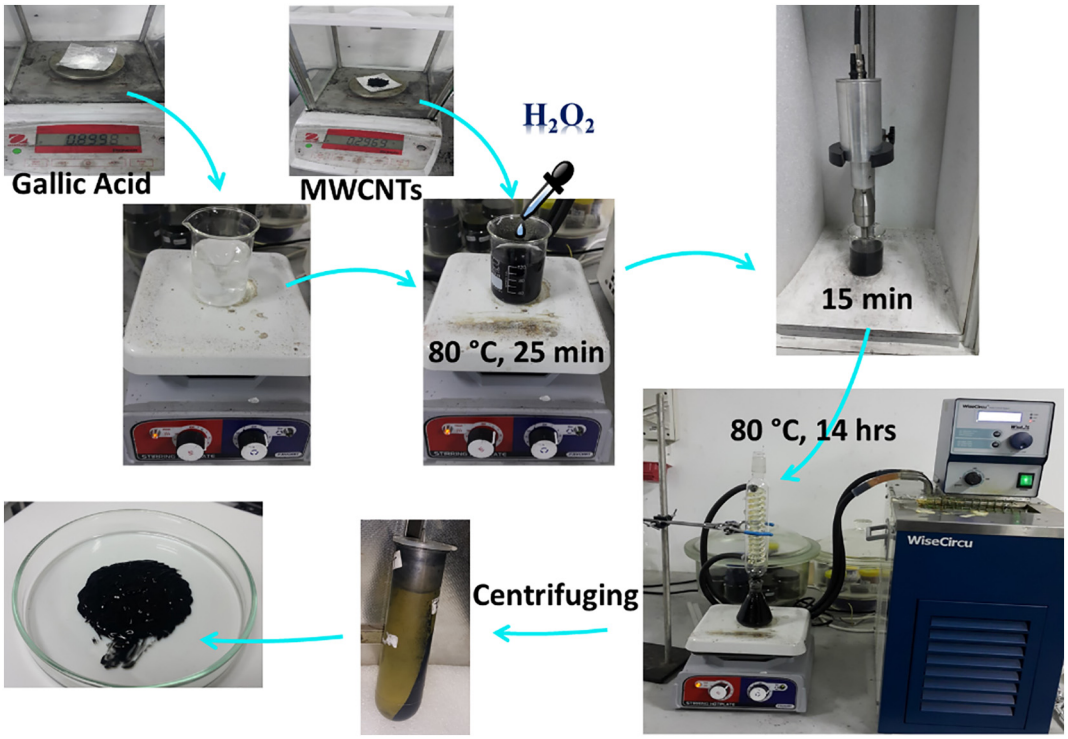


**Fig. 1.** Synthesis of the GAMWCNTs.

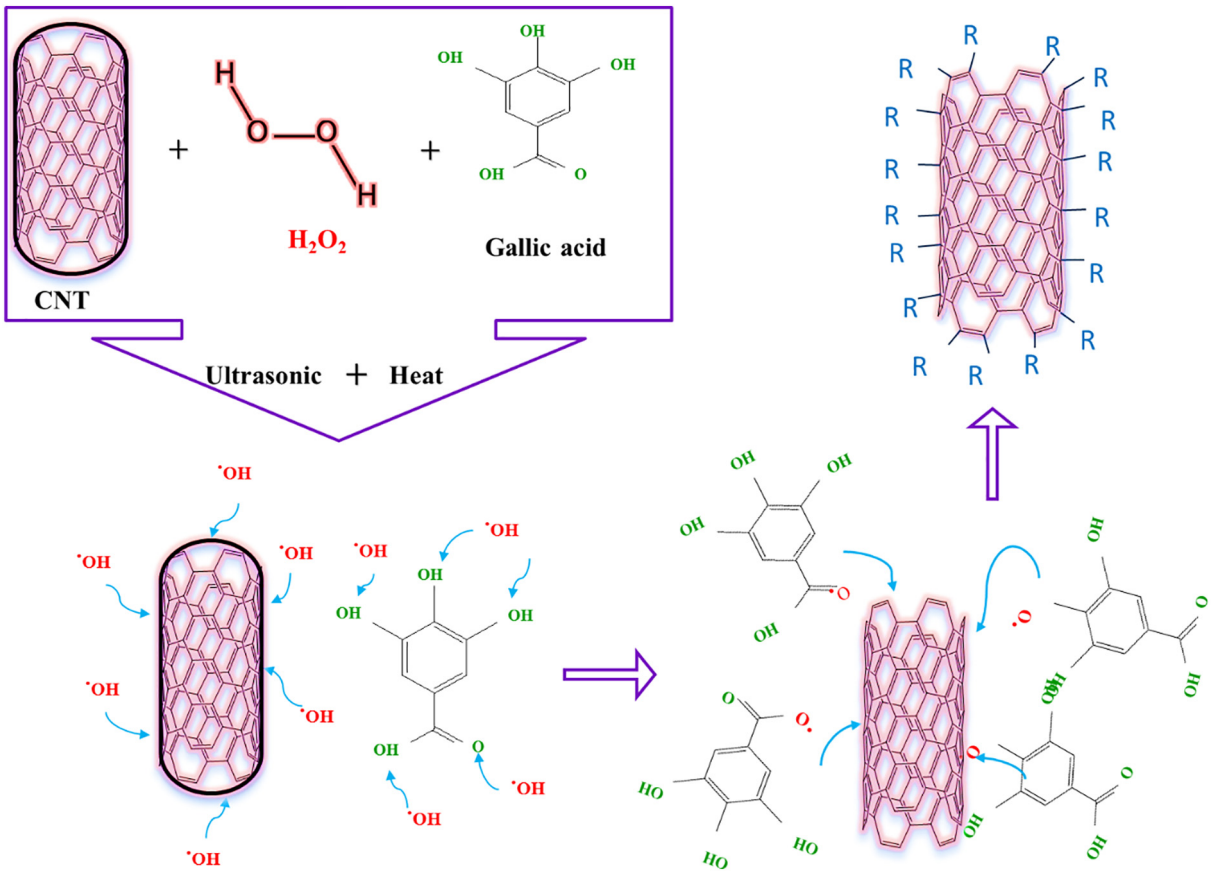


**Fig. 2.** Schematic of the functionalization procedure of MWCNTs with gallic acid.

of MWCNTs. The hydroxyl radicals can attack the CNTs directly, leading to the formation of hydroxyl groups on the CNTs surface [40].

### 2.3. Experimental procedure

Th experimental procedure comprises several steps. First, the nanofluids were produced and then the thermophysical properties of the nanofluids were assessed for the base fluid and synthesized nanofluids. Different analytical equipment was used to characterize the nanomaterials, base fluid, and nanofluids. Finally, the closed conduit was used to investigate the heat transfer and frictional properties of nano-coolants.

Ultrasonication was carrying out using an ultrasonic liquid processor (Misonix Inc., USA) having an output up to 600 W. Hitachi HT7700 transmission electron microscope (high-resolution digital TEM) was employed to test the morphological properties of the pristine and functionalized MWCNTs. Prior to TEM, the samples were prepared by ultrasonically dispersing the functionalized MWCNTs in ethanol before collection on Lacey carbon grids. The Zetasizer Nano ZS two-angle particle and molecular size analyzer (Malvern Instruments Ltd., UK) was utilized to estimate the zeta potential of the samples. The UV-1800 Ultraviolet–visible spectrophotometer (UV/VIS spectrometer) (Shimadzu Corporation, Japan) was employed to examine the dispersibility and stability of the nanofluids. To enable detectable wavelengths for the UV/VIS spectrometer to pass through the aqueous nanofluids, DI water was used to dilute the samples with a ratio of 1:20. Using special quartz cuvettes suitable for UV region, the light absorbance of all samples was measured at different time intervals over the course of 63 days. The effective thermal conductivity of the nanofluids was measured using KD-2 Pro thermal properties analyzer (Decagon Devices, Inc., USA) with KS-1 probe sensors (length: 6 cm, diameter: 1.3 mm). The accuracy of the thermal conductivity measurement was about 5%. To ensure equilibrium of the nanofluids, an average of 16 measurements was recorded over a 4-h period for each temperature and nanoparticle weight concentration. The instrument was calibrated using DI water as the base fluid before measuring the thermal conductivity of the nanofluids. The thermal conductivity of DI water was measured at 30 °C and the value was found to be 0.609 W/m·K, which are in good agreement with those obtained in previous studies [41,42]. The Physica MCR rheometer (Anton Paar GmbH, Austria) was utilized to measure the dynamic viscosity of the aqueous nanofluids. The rotary rheometer comprising a cylindrical moving platform and a steady cylindrical surface parallel to a tiny gap. The sample density was analyzed via DE-40 density meter (Mettler Toledo GmbH, Switzerland) with a precision of $10^{-4}$ g/cm$^3$.

The general experimental setup for convective heat transfer includes a horizontal pipe as the test section, a pump, reservoir tank, cooling unit, data acquisition system, a heated test section, and measuring instruments (including a flow meter and differential pressure transmitter (DPT). The experimental setup used in this study is displayed in Fig. 3. In addition, a 10-L stainless steel jacket tank with pump (Araki Axis EX-70 R) was used for the aqueous nanofluids with a flow rate of 0–14 L/min. Foxboro differential pressure transmitter and SE 32 inline paddle wheel transfer transmitter (Bürkert Contromatic Corp., USA) with display were used to evaluate the pressure loss and flow rate, respectively. The pump flow was regulated using Hoffman Muller inverter. A straight, seamless, stainless steel tube (outer diameter: 12 ± 0.1 mm, length: 1400 mm, inner diameter: 10 mm) was used as the experimental test section. An ultra-high-temperature flexible tape heater (width: 12.5 mm, length: 3.6 m) was carefully wrapped surrounding the test section at a maximum power of 940 W to prepare the final heated section of 1.2 m. The heater wires were linked to a QPS VT2–1

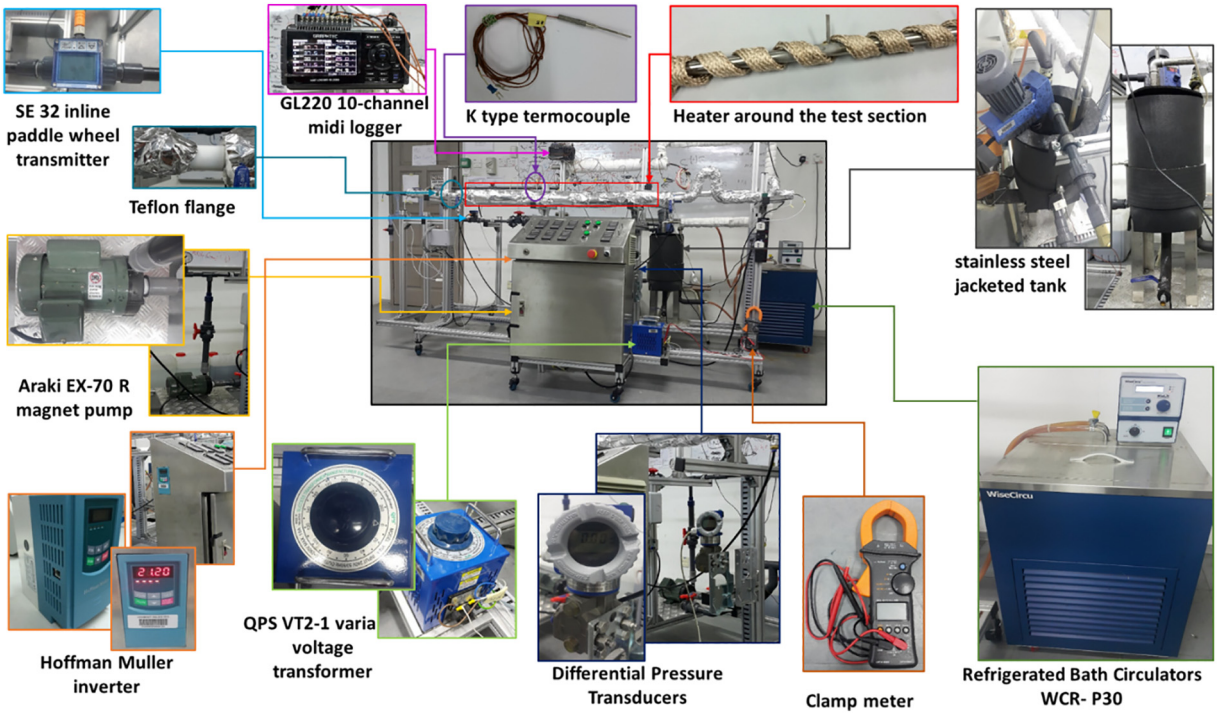


**Fig. 3.** Photographs of the experimental setup used to measure the convective heat transfer of a closed conduit where GAMWCNT-water nanofluids were utilized as the operating fluid.

variable voltage transformer (Success Electronics & Transformer Manufacturer Sdn. Bhd., Malaysia).

The voltage and current were measured by 1000 A true RMS clamp meter (Agilent) to set the desired heating power. Five K-type thermocouples were inserted into stainless steel thermocouple sleeves, which were installed on the upper surface of the test section by using high-temperature epoxy glue. The axial distances of the thermocouples from the test tube inlet were 20, 40, 60, 80, and 100 cm. Two platinum resistance temperature sensors (Pt-100 RTDs) were used in the stream of the tube inside at the outlet and inlet positions of the test rig to measure the bulk flow temperature. The maximum error of the thermocouples was ±0.2 °C. To track and record the temperature values, the thermocouples were linked to the GL220 10-channel digital logger (Graphtec Corporation, Japan). The test section was wrapped with thick fiberglass wool for the purpose of reducing heat loss to the surroundings as well as to achieve steady-state temperature at the inlet and outlet of the test section.

Table 1 Provides the accuracy and specifications of the measuring devices and sensors utilized in the present experimental setup.

### 2.4. Data processing

The values obtained from experiments were processed to analysis the heat transfer and hydrodynamic behavior of an innovative eco-friendly functionalized-MWCNT nano-coolant in a closed conduit system. By considering the pipe wall conduction and convection heat transfer by the fluid flow in the experimental test section, calibration is crucial to determine the temperature of the interior surface of the tube. Therefore, the Wilson plot technique [43] was used, which equates the resistance between various sections of the heat transfer direction and measuring the internal surface temperatures of the pipe via mathematical formulation. To study the effect of the GAMWCNT aqueous suspensions on the thermal properties of the base fluid, the significant parameters, namely, the convective heat transfer coefficient ($h$), pressure drop (DP), and $Nu$ need to be assessed. The coefficient of convective heat transfer was measured from the experimental values including the measured surface, bulk, and outlet and inlet temperatures using Newton's cooling law:

$$h = \frac{q''}{(T_w - T_b)} \tag{1}$$

In Eq. (2), the wall temperature, bulk, and heat flux are represented by $T_w$, $T_b$, and $q''$, respectively. In addition, $T_b$ is calculated as $(T_o + T_i)/2$, where $T_i$ and $T_o$ denote the inlet and outlet temperatures of the working fluid, respectively. Eq. (2) is used to measure the heat flux:

$$q'' = \frac{Q}{A} \tag{2}$$

**Table 1**
Specifications and errors of the measuring instruments and sensors utilized in the current experiment.

| Measured parameter | Devices and sensor type | Working condition | Error |
|---|---|---|---|
| Surface temperature | K-type thermocouple | 0–300 °C | ±0.1 °C |
| Bulk temperature | RTD (PT-100) sensor | 0–200 °C | ±0.1 °C |
| Flowmeter | Bürkert ceramic paddle wheel | 0.03–12.00 m/s | ±0.5% |
| Pressure drop | ALIADP differential pressure transmitter (DPT) | 0–25 kPa | ±0.075% |
| Cooling unit | WiseCircu DAIHAN Scientific Refrigerated circulating bath | 2.2 kW | ±0.1 °C |

where the input power ($Q = VI$) provided by the power supply and $A$ the internal surface area of the heated pipe is defined as $\pi DL$.

The input power of 600 W was used in this experiment which is calculated as $VI$. The $Nu$ can be determined using Eq. (3) as follows:

$$Nu = \frac{h \times D}{K} \tag{3}$$

where h, K, and D are defined as the convective heat transfer coefficient, thermal conductivity, and the inner diameter of the tube, respectively. The Reynolds number ($Re$) was measured via the following equation:

$$Re = \frac{\rho v D}{\mu} \tag{4}$$

here velocity, density, and dynamic viscosity of the operating fluid are $v$, $\rho$, and $\mu$, respectively.

The empirical correlations for Nusselt number for single-phase fluids were proposed by Gnielinsky [44], Petukhov [45], and Dittus Boelter [46], respectively, are as follows:

$$Nu = \frac{\left(\frac{f}{8}\right)(Re - 1000)Pr}{1 + 12.7\left(\frac{f}{8}\right)^{0.5}\left(Pr^{\frac{2}{3}} - 1\right)} \tag{5}$$

Where $Pr$, $Re$, and $f$ is the Prandtl number ($Pr$), Reynolds number ($Re$), and the friction factor, respectively. Eq. (5) is acceptable for the following range: $0.5 < Pr < 2000$ and $3 \times 10^3 < Re < 5 \times 10^6$.

$$Nu = \frac{\left(\frac{f}{8}\right)RePr}{1.07 + 12.7\left(\frac{f}{8}\right)^{0.5}\left(Pr^{2/3} - 1\right)} \tag{6}$$

Eq. (6) is useful for the range of $3000 < Re < 5 \times 10^6$ and $0.5 < Pr < 2000$.

$$\mathrm{Nu} = 0.023\ \mathrm{Re}^{0.8}\mathrm{Pr}^{0.4} \tag{7}$$

Eq. (7) is applicable for the range of $0.6 < Pr < 200$ and $Re > 10^4$.

The friction factor, in Eqs. (5), (6) is determined by Petukhov [45] as:

$$f = (0.79\,Ln\ Re - 1.64)^{-2} \tag{8}$$

For $2300 < Re < 5 \times 10^6$. The pressure drops across the test section measured from experiments was used to determine the friction factor of the DI water and GAMWCNT/water nanofluids using Eq. (9):

$$f = \frac{\Delta P}{\left(\frac{L}{D}\right)\left(\frac{\rho v^2}{2}\right)} \tag{9}$$

where $v$ and $\Delta P$ denote the flow velocity and pressure drop, respectively.

Eqs. (8), (10) represent the empirical correlations for the friction factor of the base fluid proposed by Petukhov [45] and Balsius [47], respectively.

$$f = 0.3164\ \mathrm{Re}^{-0.25} \tag{10}$$

Eq. (10) is useful for the following range: $3000 < Re < 5 \times 10^5$.

Eq. (11) is used to measure the pumping power for the turbulent flow regime [48]:

$$\dot{W} = 0.158\left(\frac{4}{\pi}\right)^{1.74}\left(\frac{L\dot{m}\,2.75\mu^{0.25}}{\rho^2 D^{4.75}}\right) \tag{11}$$

here $\dot{m}$ is the mass flow rate.

By using $\rho = \frac{\dot{m}}{V}$ and $v = \frac{\dot{V}}{A}$ for a constant $\mathrm{Re} = \frac{\rho v D}{\mu}$ and substituting $\dot{m}$ into Eq. (11) [49], the relative pumping power $(\frac{\dot{W}_{nf}}{\dot{W}_{bf}})$ for a fixed $Re$ is provided as follows:

$$\frac{\dot{W}_{nf}}{\dot{W}_{bf}} = \left(\frac{\rho_{bf}}{\rho_{nf}}\right)^2\left(\frac{\mu_{nf}}{\mu_{bf}}\right)^3 \tag{12}$$

where $\dot{W}_{bf}$ and $\dot{W}_{nf}$ denote the pumping power of the water and GAMWCNT aqueous nanofluids, respectively [6].

The performance index of the convective heat transfer system can be determined using Eq. (13) [6]:

$$\varepsilon = \frac{h_{nf}/h_{bf}}{\Delta P_{nf}/\Delta P_{bf}} = \frac{R_h}{R_{\Delta P}} \tag{13}$$

Here, $R_{\Delta P}$, $R_h$is the ratio of pressure drop and convective heat transfer enhancement.

The uncertainty analysis of the measured data containing Nusselt number, heat transfer coefficient, friction factor and Reynolds number are carrying out based on the procedure of Taylor and Thompson [50], and Kline and Mcclintock [51]. The uncertainty of parameter R can be determined using Eq. (14) as follows:

$$U_R = \sqrt{\sum_{i=1}^{n}\left(\frac{\partial R}{\partial V_i}U_{V_i}\right)^2} \tag{14}$$

Where $U_R$ and $U_{Vi}$ denote the uncertainties related to the parameter R and independent variable $V_i$, respectively. In addition, n is the number of independent variables. The uncertainty values calculated using Eq. (14) and the results are represented in Table 2.

## 3. Results and discussion

### 3.1. Materials characterization

The FTIR spectra of pure MWCNTs and GAMWCNTs are displayed in Fig. 4(a). The GAMWCNT sample demonstrates clear evidence of the presence of various functional groups compared to that of the pure MWCNTs. The sharp and broad peaks at 3446–3750 $cm^{-1}$ are associated with the O–H stretching vibrations at the main structure of both MWCNTs and GAMWCNTs with different intensities. The reason behind this is because of the reaction between the MWCNTs and hydroxyl (O–H) groups of gallic acid (GA) and/or hydrogen peroxide ($H_2O_2$). Moreover, both GAMWCNTs and MWCNTs are given symmetric and asymmetric peaks in a range of 2850–3000 $cm^{-1}$ which are ascribed to the C–H bonds. It can be observed from Fig. 4(a) that a peak centered at a wavenumber of 2360 $cm^{-1}$ in the spectrum of the GAMWCNTs corresponds to $CO_2$ [52]. Moreover, a couple of peaks at 1388 and 1562–1639 $cm^{-1}$ are assigned to $CH_2$ bending vibrations and C=C stretching vibrations of MWCNTs after opening owing to the addition of electrophilic reactions between the main structure of MWCNTs and the –OH band of GA, respectively. In accordance with the FTIR spectrum, the GA is successfully connected to the pure MWCNTs via free-radical grafting reaction.

**Table 2**
Uncertainty analysis data for the convective heat transfer experiment.

| Variable name | uncertainty range |
|---|---|
| Reynolds number, *Re* | ±2.23% |
| Convective Heat transfer coefficient, h | ±1.11137% |
| Nusselt number, *Nu* | ±3.55% |
| Friction factor, f | ±1.39168% |

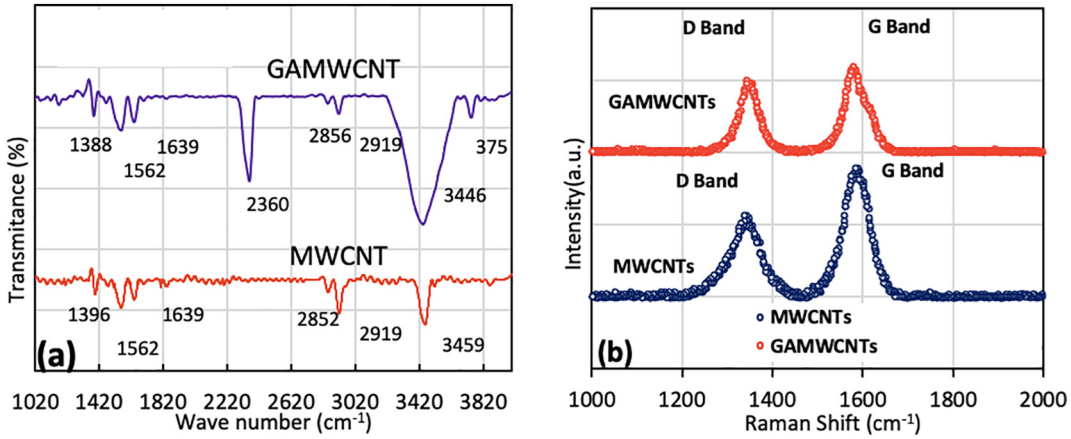


**Fig. 4.** (a) FTIR spectra and (b) Raman spectra for pristine MWCNTs and GAMWCNTs.

Raman spectroscopy is now an increasingly important method for characterizing carbon-based materials. In addition to its non-destructive nature, it is simple and relatively sensitive not only to the crystal structure, but also to the structural changes at the molecular level. As a result, Raman spectroscopy thus has a strong ability for the assessment of chemical functionalization. The Raman spectra of the GAMWCNTs and pristine MWCNTs are shown in Fig. 4(c). What can be seen in this figure is that both the pristine MWCNTs and GAMWCNTs have D and G bands at a wavenumber of ~1350 and 1590 $cm^{-1}$, respectively. The D and G bands are associated with amorphous carbon/disordered carbon ($sp^3$) and graphitic carbon ($sp^2$), respectively. A higher $I_D/I_G$ rate means that owing to covalent functionalization, the number of $sp^2$ hybridized carbons changed to the $sp^3$ hybridization carbons. The $I_D/I_G$ ratio was found to be 0.62 and 0.71 for the MWCNTs and GAMWCNTs, respectively. The elevated $I_D/I_G$ ratio of the GAMWCNTs was due to the increased number of $sp^3$ carbon and the occurrence of electrophilic addition reaction. The complete data of Raman spectra analysis are given in Table 3.

Despite that the TEM imaging does not provide any details on the functional groups, this technique makes it possible to examine the alteration on the MWCNT surface, which serves as supplementary proof of successful covalent functionalization. Fig. 5(a–b) illustrates the TEM pictures of the pristine MWCNTs and GAMWCNTs. The cut and open ends of the GAMWCNTs are evident, which might be a result of the partial damage of graphitic (sp2) carbon after covalent functionalization in which the carboxylation stages and replacement of carboxyl groups occurred. The defects are the places to characterize GA in the main structure of the MWCNTs. As the defects increase in the structure, the carboxylic groups (defects) in the structure of the MWCNTs considerably increase the stability of MWCNTs in the base fluid. The measured zeta potential data of GAMWCNT with respect to the pH are shown in Fig. 5(c). The GAMWCNTs show high negative values in the range of −16 to −52.4 mV for a pH range of 2.70–9.56, where the values are far from the point of isoelectric. In the pH range of 3.10–9.56, the GAMWCNTs have strong electrostatic repulsion force, which prevents the MWCNTs from aggregation by noncovalent interactions like π-π interactions or H-bonding. The oxygen functional groups at the surface of the MWCNT are responsible for this phenomenon. The aqueous suspensions of GAMWCNT are thus stable at a pH above 3.1, with a zeta potential of about −32.1 mV. It shall be highlighted that in this work, the GAMWCNT/water colloidal suspensions are well-stable in even slightly acidic conditions. The material appears to agglomerate in more acidic solutions (pH < 3.1) and undergoes intermolecular dehydration catalyzed with H+, which contributes toward coupling of the GAMWCNTs through the ether connections. By adding alkaline to the aqueous suspension, which leads to an additional negative charge in the nanoparticles, the GAMWCNT nanofluid is more stable.

**Table 3**
Raman spectra analysis results for the pristine MWCNTs and GAMWCNTs.

| Sample | Peaks | Center ($cm^{-1}$) | Intensity (a.u.) | $I_D/I_G$ |
|---|---|---|---|---|
| Pristine MWCNTs | D band | 1344.989 | 1117.054 | 0.63 |
| | G band | 1594.618 | 1777.089 | |
| GAMWCNTs | D band | 1352.577 | 1308.141 | 0.71 |
| | G band | 1587.16 | 1836.491 | |

Ultraviolet–visible spectroscopy analysis is a typical procedure used to investigate the stability of nanoparticle aqueous suspensions. The Beer-Lambert law states that there is a direct connection between the absorbance of a colloidal suspension and the mass fraction of the absorbing species like particles in a suspension. Following this law, the absorption spectrum of the prepared aqueous nanofluids displayed a maximum peak at around 260 nm, which corresponds to $\pi - \pi$ transition of conjugation system in the polyaromatic structures.

A typical method of stabilizing aqueous suspensions for nanoparticles is the UV/VIS spectrum analysis. The Beer-Lambert law states that the absorption of a colloidal dispersion is specifically related to the mass fraction of absorbent species, like suspended solids particles in the solution. Under this rule, there was a maximum absorption range of 260 nm of the synthesized nanofluids, which correlates to a π–π conjugation mechanism transformation in the polyaromatic structures.

UV/VIS spectroscopy analysis was conducted for the GAMWCNT/water nanofluids at various nanoparticle concentrations and photometric analysis was employed to examine the variation of relative weight fraction of the samples versus time (number of days after preparation). The UV/VIS spectra for the GAMWCNT/water nanofluids are shown in Fig. 6(a). The absorbance peak values for all of the samples were located at 260 nm, which is attributed to the presence of GAMWCNTs. Moreover, the absorbance of the GAMWCNT aqueous nanofluids decreased as the nanoparticle concentration decreased from 0.1 wt% to 0.025 wt %, indicating that increasing the amount of the dispersed GAMWCNTs will increase the absorbance value. As shown in Fig. 6(b), there is a strong linear relationship between the concentration of GAMWCNTs and the absorbance, which conforms to Beer's law, indicating that the functionalized GAMWCNTs are well dispersed in the base fluid.

Fig. 6(c) shows the variation of colloidal stability of the GAMWCNT aqueous nanofluids as a function of the number of the days after preparation. What can be clearly seen in this figure is the relative concentration of GAMWCNT aqueous nanofluids decreases with the number of the days after preparation. In spite of the fact that the relative concentration of the GAMWCNT aqueous nanofluids remained steady after Day 45. The maximum magnitude of sedimentation was reported

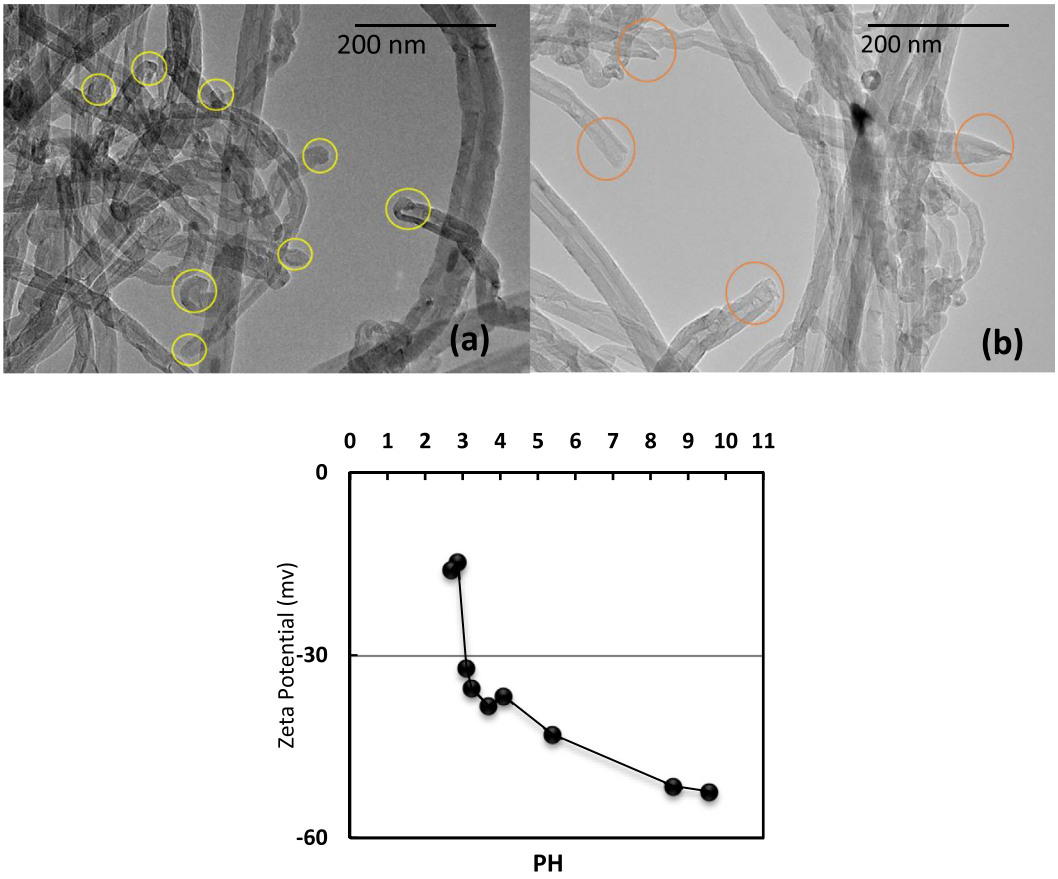


**Fig. 5.** (a, b) TEM pictures of pure MWCNTs and GAMWCNTs, and (c) zeta potential data of GAMWCNT aqueous nanofluids against pH values.

8.00, 9.33, and 10.9% for a weight fraction of 0.025, 0.075, and 0.1%, respectively. This certifies the stability of the synthesized nanofluids.

### 3.2. Thermophysical properties of GAMWCNTs aqueous suspensions

Fig. 7(a) shows the effective viscosity of GAMWCNT aqueous nanofluids and DI water. It is evident that the effective dynamic viscosity is dependent on the temperature and weight concentration at specific shear rate of 150 $s^{-1}$. The dynamic viscosity of the samples only increased slightly when the GAMWCNTs were loaded relative to the dynamic viscosity of DI water. This phenomenon is anticipated because our samples used only a small weight fraction of GAMWCNTs [6]. This slight increase in viscosity also indicates the benefit of using the covalent functionalization method rather than using the noncovalent functionalization method including surfactants such as gum arabic, triton X-100, sodium dodecylbenzene sulfonate surfactant (SDBS), which leads to a higher viscosity of corresponding nanofluids. Moreover, the GAMWCNTs remain more suspended in the DI water. According to a previous study [53], poor dispersibility and consequently increasing agglomeration size will directly promote the viscosity of nanofluids. In addition, the Fig. 7(a) shows that the dynamic viscosity of the GAMWCNT aqueous working fluids decreases as the temperature increases, which might be a result of the weakening of intermolecular forces between the GAMWCNT particles [54–56].

This observation are in agreement with the results of Aravind et al. [54], Sadri et al. [57], Ko et al. [58], and which showed the viscosity decreased with a growth in the fluid temperature. The slight increase in the effective viscosity with an increase in the nanoparticle concentration is a major benefit of the GAMWCNT/water nanofluids since a higher effective viscosity can undermine the useful effect of the higher thermal conductivity of the nanofluids owing to the increase in pumping power, which is detrimental for heat transfer systems. Keblinski, Phillpot, Choi, & Eastman [59] and Jeffrey A. Eastman, Phillpot, Choi, and Keblinski [60] have proposed four possible mechanisms to explain the reasons for increasing the thermal conductivity of nanofluids including liquid molecular level layering at the interface between fluid and particles, nanoparticles Brownian motion, the nature of nanoparticle's thermal transport, nanoparticles cluster impacts. The thermal conductivity of a coolant plays an important role in rising the rate of heat transfer in heat exchangers. Therefore, in this work, the thermal conductivity of the GAMWCNT aqueous working fluids was assessed experimentally and the outcomes are represented as a function of temperature and nanoparticle weight concentration, as shown in Fig. 7(b). Low concentrations of GAMWCNTs have been taken into consideration in this work to prevent an increase in the dynamic viscosity. In comparison with that in the database of the National Institute of Standards and Technology (NIST), the thermal conductivity of the DI water as the base fluid was found to be consistent [61], with less than 1% deviation. What can be clearly seen in Fig. 7(b) is that the thermal conductivity of the nanofluids is remarkably higher than that for the base fluid. In addition, it is clear that the thermal conductivity of both the nanofluids and DI water increase with a growth in the fluid temperature. However, the increase in thermal conductivity is greater for the nanofluids at higher nanoparticle concentrations. It can be deduced from Fig. 7 (b) that the thermal conductivity of the nanofluids is a significant factor in increasing the Brownian movement of nanoparticles dispersed in the base fluid (e.g. water). [54]. The highest increase in nanofluid thermal conductivity achieved was 5.024, 14.130, and 21.510% for a weight fraction of 0.025, 0.075, and 0.1% at 45 °C.

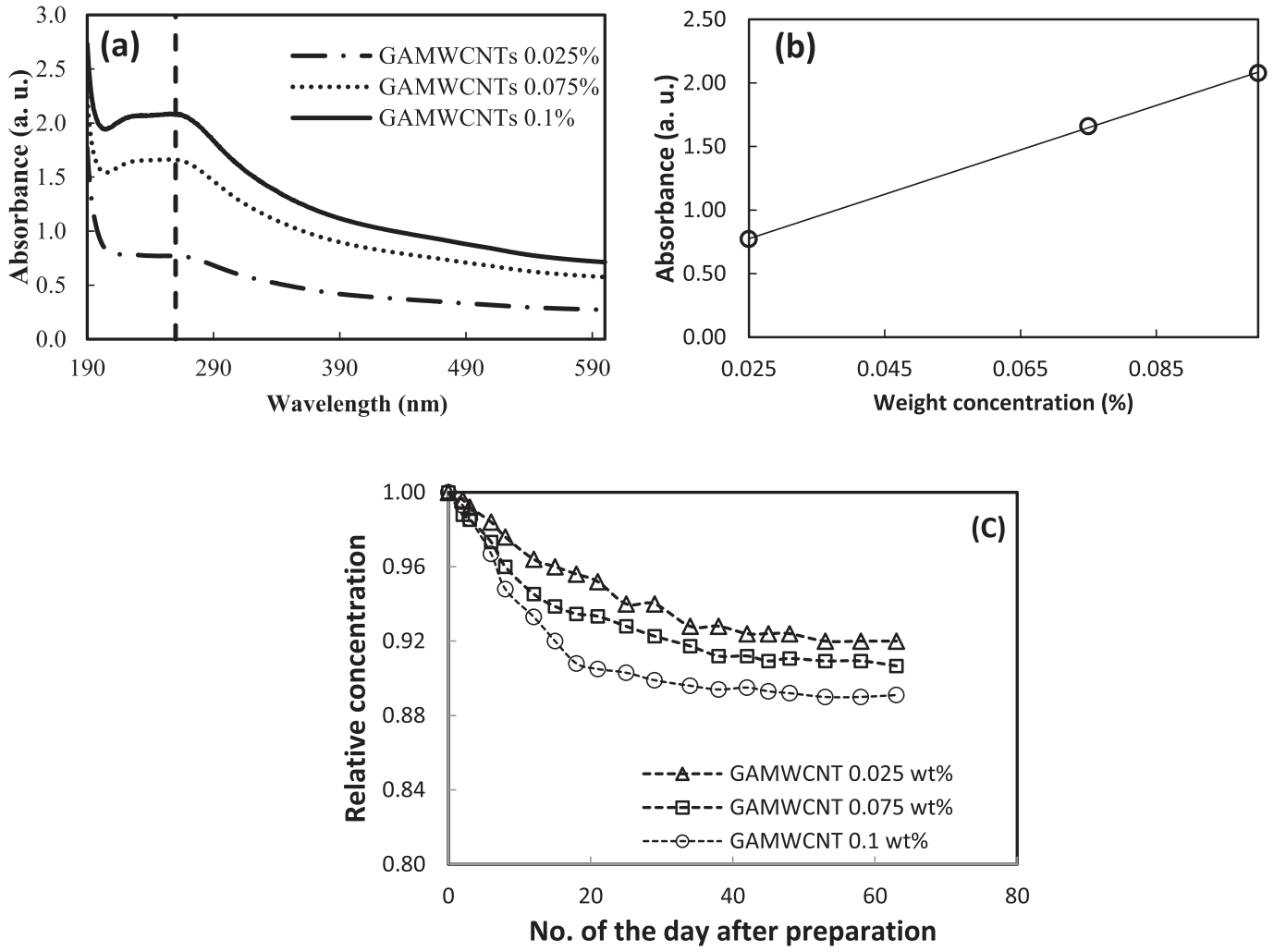


**Fig. 6.** (a) UV/VIS spectroscopy analyses of the GAMWCNT aqueous nanofluids at diverse wavelengths and nanoparticle concentrations. (b) Absorption values of the GAMWCNTs dispersed in DI water at diverse nanoparticle concentrations. (c) Colloidal stability of the GAMWCNTs suspended in water at diverse nanoparticle concentrations.

The specific heat capacity of the GAMWCNT nanofluids as a function of the nanoparticle concentration and fluid temperature is shown in Fig. 7(c). The specific heat capacity for DI water was also plotted in the same graph for comparison. What can be seen in the Fig. 7(c) is that the specific heat capacity of the GAMWCNT nanofluids decreases by enhancing the weight fraction of the GAMWCNTs, where the average reduction in the specific heat capacity was 0.33–1.42% compared with those for DI water, and this is only a marginal decrease. This reduction is attributed to the reduced specific heat capacity of the GAMWCNT aqueous nanofluids compared with that of the base fluid.

The experimental values of the dynamic viscosity for the GAMWCNT aqueous nanofluids were compared with those calculated using the empirical correlations of Batchelor [62] and Einstein [63] (Eqs. (14, 15), respectively) and the results are presented in Fig. 8. The experimental values were consistent with those calculated from the correlational analysis with a maximum error of ~7% for the GAMWCNT/water nanofluids. It is crucial to reduce the increment in viscosity of heat transfer working fluids by using an appropriate synthesis method. Considering the low nanoparticle concentrations for the GAMWCNT/water nanofluids in this work, particularly for heat transfer systems, in where the overall positive impact in heat transfer is not undermined by the pumping fluid penalty because there is only a minor increase in viscosity [64,65]. Hence, to maximize the heat transfer performance of closed-loop systems in which nanofluids are used as the working fluids, it is imperative to maintain the resultant colloidal mixtures in Newtonian behavior since this will reduce the pumping power compared to non-Newtonian fluids.

$$\text{Batchelor model}: \frac{\mu_{nf}}{\mu_{bf}} = 1 + 2.5\varphi + 6.5\varphi^2 \tag{14}$$

$$\text{Einstein model}: \frac{\mu_{nf}}{\mu_{bf}} = 1 + 2.5\,\varphi \tag{15}$$

where $\mu_{nf}$, $\mu_{bf}$ and $\varphi$ is the viscosity of the nanofluid, the viscosity of the base fluid, and the volume fraction of the nanoparticles, respectively.

The density was experimentally tested for the GAMWCNT aqueous nanofluids and water at a variety of temperature, and outcomes are set out in Table 4. It can be observed that there was a drop in the density for both the aqueous nanofluids and DI water as the fluid temperature increased due to thermal expansion of liquid. In addition, there was a slight increase in the density of all nanofluids as the nanoparticle concentration was increased. The observed increase in density may be related to the density of the GAMWCNTs, which is higher than that for water. Thereupon, an increase in particle loading will lift the density of the nanofluids suspensions. The maximum increase in density of the GAMWCNT aqueous nanofluids was 0.055% for a weight fraction of 0.1% at 35 °C. In addition, the density dropped for the same nanoparticle concentration by 0.6% as the fluid temperature was raised from 20 °C to 40 °C.

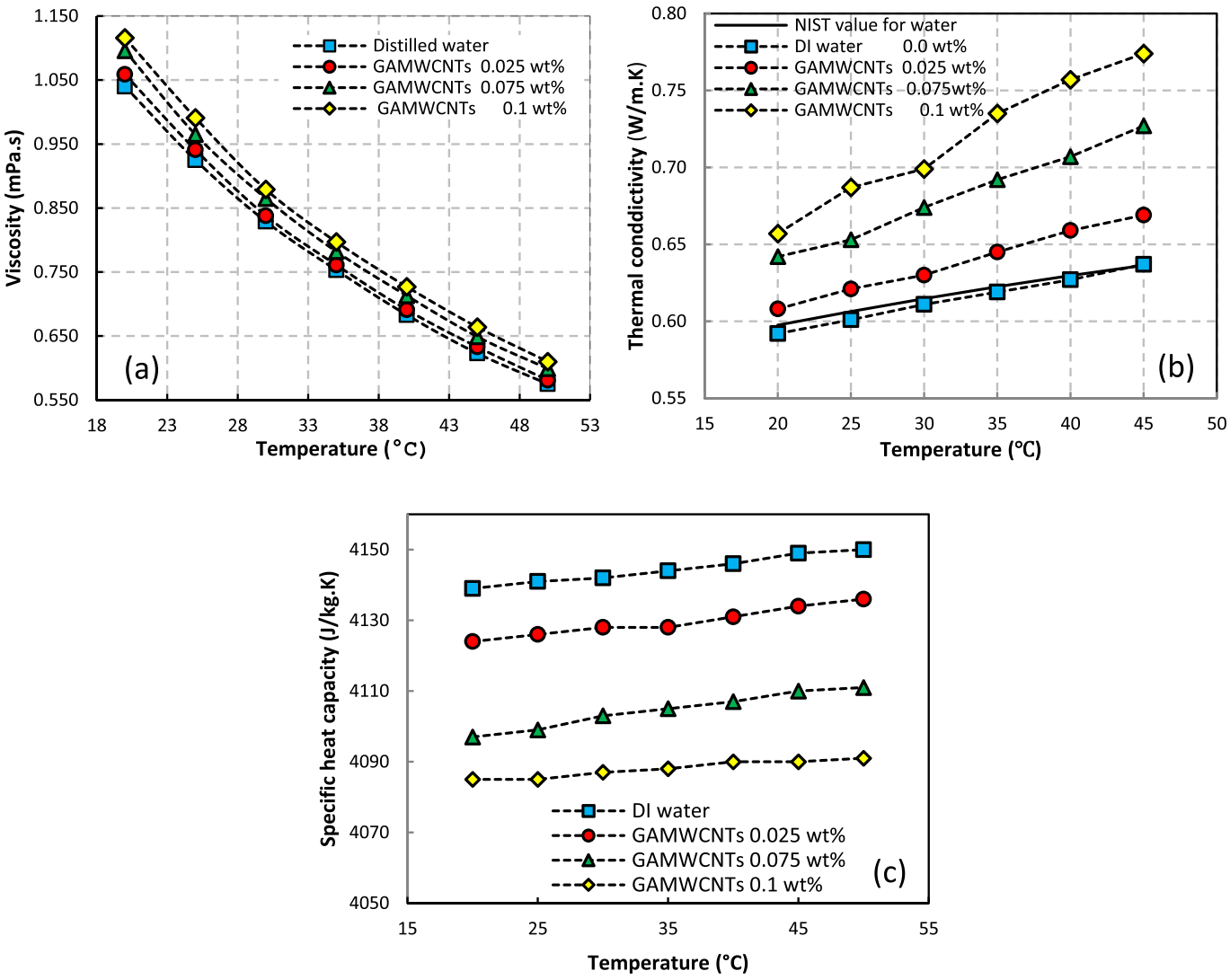


**Fig. 7.** Variations of the (a) dynamic viscosity, (b) effective thermal conductivity, and (c) specific heat capacity of GAMWCNT aqueous working fluids at diverse temperatures and weight concentrations.

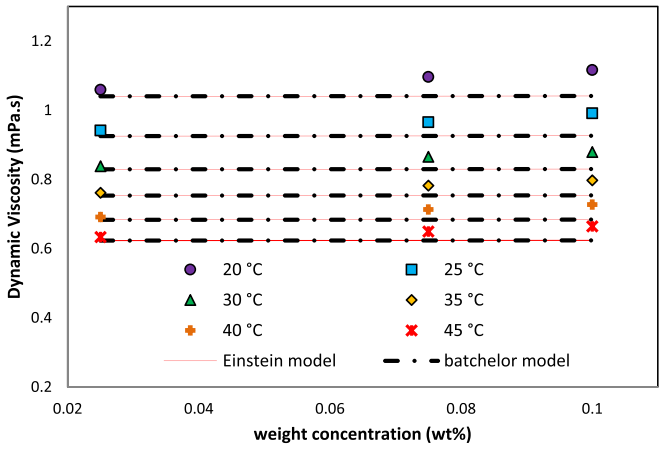


**Fig. 8.** Dynamic viscosity values of the GAMWCNT aqueous nanofluids compared with those calculated by theoretical models with respect to the nanoparticle wight concentration and temperature at a shear rate of 150 $s^{-1}$.

### 3.3. Heat transfer and hydrodynamic characteristics

The average *Nu* obtained from experiment was compared with those evaluated from the empirical correlations of Dittus-Boelter [46], Petukhov [45], and Gnielinski [44]. The *Nu* increased when the *Re* increased, as shown in Fig. 9(a). Furthermore, the experimental *Nu* values were consistent with the values obtained from empirical correlations. The average error between the experimental values and those obtained from the correlations of Dittus-Boelter [46], Petukhov [45], and Gnielinski [44] were 7.96, 2.01, and 7.11%, respectively. Thus, it can be

**Table 4**
The density of the DI water and GAMWCNT at diverse fluid temperature and weight fraction.

| Density (kg/m$^3$) | | | | | |
|---|---|---|---|---|---|
| Nanoparticle concentration/Fluid temperature | 20 °C | 25 °C | 30 °C | 35 °C | 40 °C |
| DI water 0 wt% | 998 | 996.85 | 995.5 | 993.9 | 992 |
| GAMWCNT 0.025 wt% | 998.1 | 997 | 995.6 | 994.05 | 992.1 |
| GAMWCNT 0.075 wt% | 998.4 | 997.25 | 995.85 | 994.35 | 992.35 |
| GAMWCNT 0.100 wt% | 998.5 | 997.35 | 995.95 | 994.45 | 992.5 |

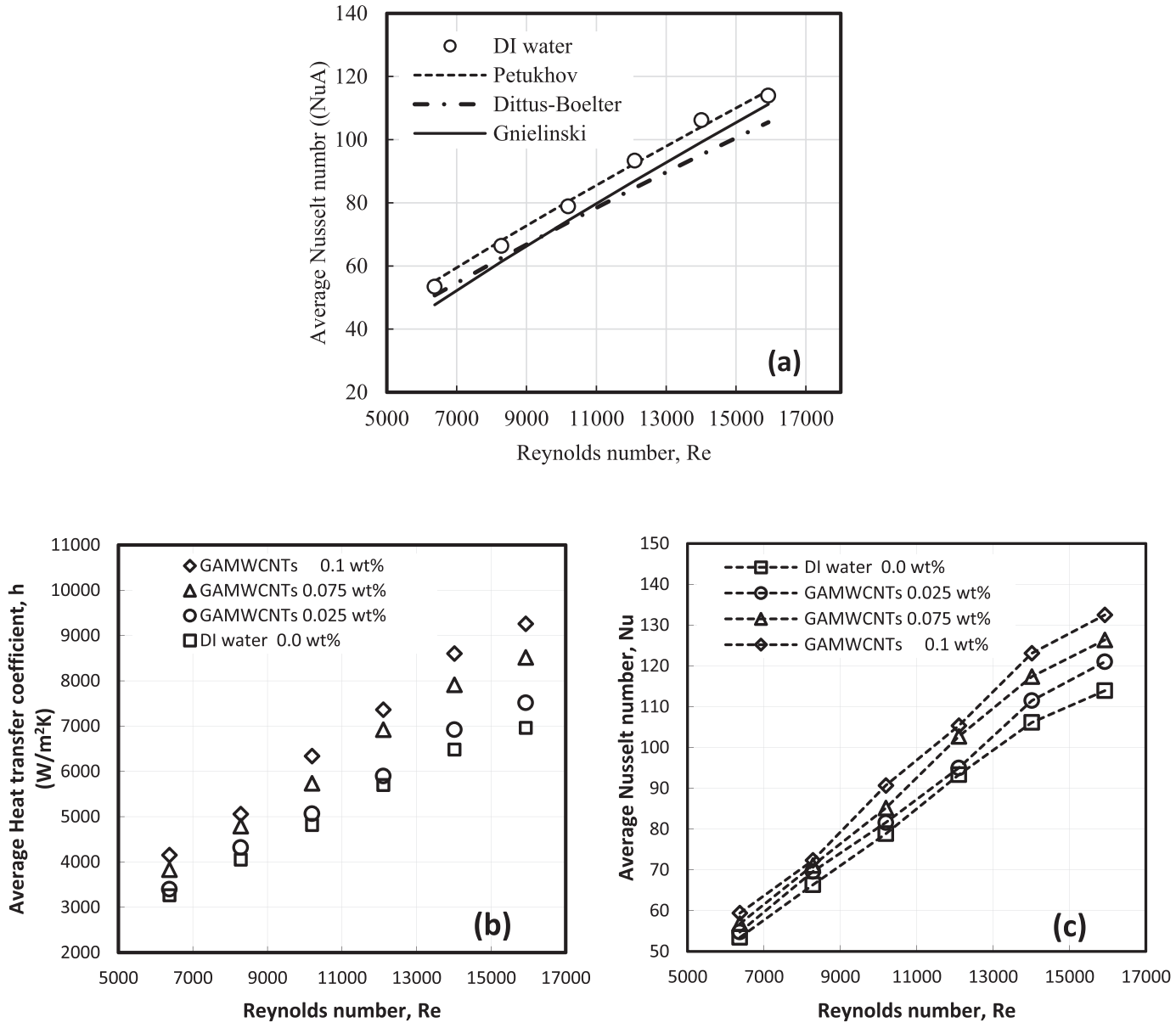


**Fig. 9.** (a) Evaluation of the *Nu* between experiments and correlational analysis for the base fluid. (b) Average heat transfer coefficient and (c) average *Nu* of the GAMWCNT aqueous nanofluids and base fluid at different *Re*.

deduced that our experimental findings correspond well to that of the empirical correlations, which shows the precision of our experimental setup for heat transfer measurements. Hence, this experimental setup can be used to assess the effectiveness of the GAMWCNT aqueous nanofluids in the improvement of heat transfer properties.

To determine the convective heat transfer coefficient of the GAMWCNT working fluids under turbulent flow regime (*Re*: 6371–15,927), different nanoparticle concentrations (0.025–0.100 wt%) were considered for the nanofluids in this study. The electrical power input was maintained at 615 W. The outcomes are set out in Fig. 9(b) at a constant inlet temperature of 30 °C. What stands out in Fig. 9(b) is the growth of convective heat transfer coefficient as the *Re* increases for both DI water and GAMWCNT-water nanofluids. It is apparent that the concentration of nanoparticle has a significant effect on the coefficient of convective heat transfer.

The notable enhancement in the convective heat transfer coefficient of the nanofluids might be related to the reduced thickness of the thermal boundary layer and the improved thermal conductivity in the existence of the GAMWCNTs, which result in a significant reduction in thermal resistance between the inner tube wall and working fluid in comparison to that of base fluid [66–69]. According to [54,70], the thickness of the thermal boundary layer tends to be reduced by carbon nanomaterials (e.g., nanoplatelets and CNTs). The Brownian motion and specific surface area (SSA) of the particles also contribute to the improvement in convective heat transfer. In the present work, the enhancement in convective heat transfer of the nanofluids was 7.94, 22.37, and 33.05% at 0.025, 0.075, and 0.1 wt%, respectively.

To evaluate the ratio of convective-to-conductive heat transfer of water-based GAMWCNT aqueous nanofluids, the average *Nu* data determined from Eq. (3) are presented in Fig. 9(c) against the *Re* and weight concentration. It can be observed that the *Nu* increases significantly as the weight fraction of GAMWCNT and *Re* increases compared to those for DI water. The improved *Nu* of the GAMWCNT/water nanofluids is attributed to the large surface area, Brownian motion, and thermophysical properties of the suspended GAMWCNTs. This further promotes the heat transport capability of the nanofluids [71]. In

addition, the improved Nu may be due to the properties of nanofluids in terms of lower specific heat and higher thermal conductivity in comparison with those of DI water. For a weight concentration of 0.025, 0.075, and 0.1, the highest improvement in *Nu* was observed to be 4.69, 10.93, and 16.30%, respectively. The maximum rise in *Nu* was achieved when $Re = 15{,}927$.

The correlations of Blasius [47] and Petukhov [45] (Eqs. (8), (10)), respectively) were utilized to compare the friction factor of DI water obtained from Eq. (9). Fig. 10 (a) displays the variation of friction factor with respect to the *Re*. The findings are promising because the highest difference between the friction factor obtained from experiment data and those acquired from the Blasius's [47] and Petukhov's [45] correlations is less than 5%. It is a demonstration of the precision and reliability of our experimental setup to estimate the pressure loss over the *Re* range investigated in this work.

The pressure drops of the GAMWCNT aqueous nanofluid flowing through the pipe was examined at different *Re* and the results are shown in Fig. 10(b). Eq. (9) was used to determine the corresponding values of friction factor, and the findings are set out in Fig. 10 (c) versus *Re*. What is striking in this figure is a minor increase in both the friction factor and pressure drop for the GAMWCNT aqueous nanofluids in comparison with that of the base fluid. The highest increment in the friction factor was found to be ~1.38, 3.00, and 3.62% at 0.025, 0.075, and 0.1 wt%, respectively. The highest increase in the friction factor was found to be ~1.38, 3.00, and 3.62% for the GAMWCNT weight fraction of 0.025, 0.075, and 0.1, respectively. This growth in friction factor is mainly attributed to the slight increase in dynamic viscosity for all nanofluids. For this reason, the velocity of the nanofluids plays an important role in increasing the pressure drop and friction factor relative to that for base fluid in forced convection heat transfer systems. This matter can be acknowledged by revisiting Eq. (9) for the friction factor and pressure drop, and Eq. (4) for the Reynolds number (*Re*). This can be confirmed by considering Eq. (9) for the friction factor and pressure drop, and Eq. (4) for the *Re*.

The power consumption and pumping characteristics of a heat transfer setup is an important factor when it comes to the energy savings and energy consumption in order to evaluate the suitability of a working fluid and optimize the energy usage of thermal equipment. The relative pumping power of the GAMWCNT nanofluids and DI water was determined using Eq. (12) and the results are presented in Fig. 11(a) as a function of the nanoparticle concentration. It shall be highlighted that Fig. 11(a) shows only a small increment in the relative pumping power up to 1.19 for the highest nanoparticle concentration (0.1 wt%). The reason behind this phenomenon might be related to the low weight fraction of the GAMWCNTs for the nanofluids in this study. Eq. (13) was used to calculate the performance index, $\varepsilon$. In this

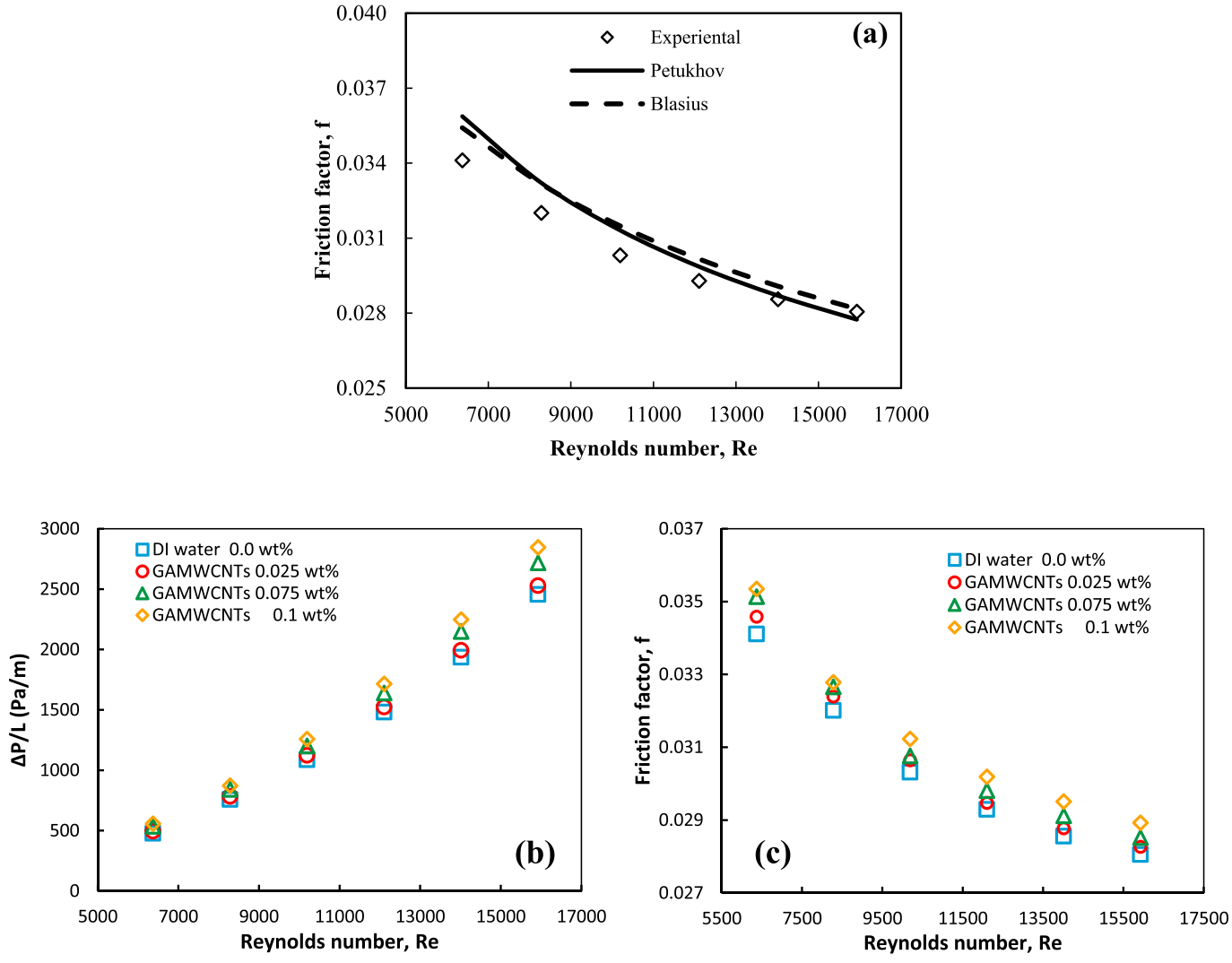


**Fig. 10.** (a) Comparison of the friction factor values obtained from experimental and empirical correlations for the base fluid. Variation of the (b) pressure drop and (c) friction factor with respect to the *Re* for the GAMWCNT nanofluid in the test section.

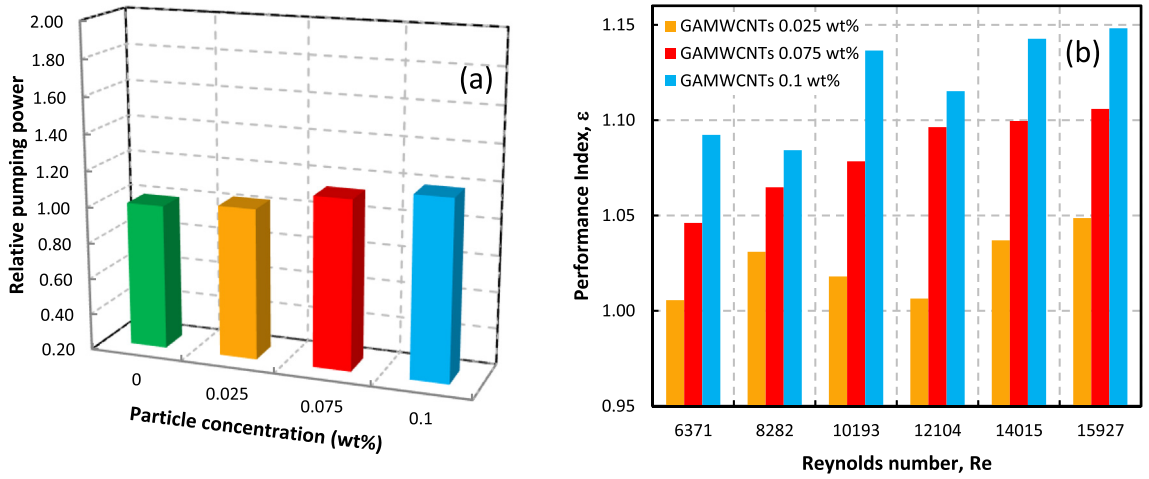


**Fig. 11.** Variation of the (a) relative pumping power against the weight concentration and (b) performance index against the Reynolds number of the GAMWCNT/water nanofluids and DI water.

work, eco-friendly GAMWCNT/water nanofluid, synthesized as a potential working fluid in heat transfer devices namely solar collectors and heat exchangers, were used to assess the economic performance.

Fig. 11(b) shows the performance index of the GAMWCNT/ water nanofluids for various nanoparticle concentrations and *Re*. The performance index for all samples was more than one and indicated the importance of using these innovative aqueous nanofluids in convective heat transfer systems. What can be clearly seen in this figure is that the performance index improves with an increase in GAMWCNT concentration in the base fluid (i.e., DI water). This signifies that loading of these eco-friendly functionalized MWCNTs in the base fluid boosts the thermal performance of the system. Fig. 11(b) indicates that, regardless of nanoparticle concentration, the Performance Index continues to increase with a grow in the *Re*. This also demonstrates that the GAMWCNT/water nanofluids can be utilized as an alternative heat transfer coolant.

## 4. Conclusion

An environmentally friendly functionalization procedure was effectively established to synthesize finely dispersed MWCNT water-based colloidal suspensions for use as coolants to improve the hydrodynamic and convective heat transfer characteristics of a straight, stainless steel heat exchanger. The following conclusions were drawn based on the findings of this study:

- The effectiveness of covalent functionalization technique was confirmed by means of characterization tests comprising FTIR spectroscopy, Raman spectroscopy, and high-resolution transmission electron microscopy.
- The stability and solubility of the functionalized MWCNT in aqueous media are confirmed via UV/Vis Spectroscopy and Zeta Potential Tests, the dispersibility value was more than 89.1% for 63 days.
- The thermal conductivity of the DI water was in good line with the NIST data [61] and the error was less than 1%. The reported improvement in the thermophysical characteristics of nanofluids compared with those for the base fluid indicates that the synthesized GAMWCNT/water nanofluids are promising coolants for convective heat transfer applications. The maximum thermal conductivity enhancement (21.51%) was achieved at the lowest nanoparticle concentration of 0.1 wt% and fluid temperature of 45 °C.
- The precision of the closed conduit heat transfer system was validated by experiments where DI water was employed as the operating fluid. The results showed that there was excellent agreement between the *Nu* obtained from experiments and those determined from Dittus-Boelters [46], Petukhov's [45], and Gnielinski's [44] theoretical correlations with a maximum deviation of 7.11, 2.01, and 7.96%, respectively. The friction factor obtained from experiments was also firmly endorsed with those determined from empirical correlations of Petukhov [45] and Blasius [47] with an average deviation of 5 and 4%, respectively.
- The results showed that there was a remarkable improvement in the convective heat transfer coefficient (~33.049%) of the GAMWCNT/water nanofluids in comparison to those for the base fluid, at a nanoparticle weight fraction of 0.1 and Reynolds number of 15,927. it is especially important that there was only a negligible increase in the friction factor up to 3.62%. These findings were provided under a turbulent flow regime with a constant wall heat flux of 12,752 W/m$^2$.
- The findings are very encouraging because the pumping power of all nanofluids prepared in this study was close to that of the DI water. Furthermore, the performance index for all samples was more than one and improved with an increase in the *Re*, which reflects the benefit of utilizing these novel nanofluids in thermal systems. The findings showed that nanofluids prepared with covalently functionalized carbon nanostructures led to a significant improvement in the heat transfer rate while the pumping power penalty was very low.

## CRediT authorship contribution statement

**Naveed Akram:** Writing – original draft, Writing – review & editing. **Maryam Hosseini:** Conceptualization, Methodology, Investigation, Writing – original draft, Writing – review & editing. **Rad Sadri:** Conceptualization, Methodology, Investigation, Writing – original draft, Writing – review & editing. **S.N. Kazi:** Supervision, Validation, Project administration, Funding acquisition, Writing – review & editing. **Alibakhsh Kasaeian:** Writing – review & editing. **Hooman Yarmand:** Writing – review & editing. **Kamel Hooman:** Writing – review & editing. **Roslina Ahmad:** Writing – review & editing.

## Declaration of Competing Interest

The authors declare that they have no known competing financial interests or personal relationships that could have appeared to influence the work reported in this paper.

## Acknowledgment

The authors take an opportunity to acknowledge the High Impact Research Grant UM.C/HIR/MOHE/ENG/45 and the University of Malaya, Malaysia, for the financial support in conducting the research work.

## References

[1] H. Togun, et al., Thermal performance of nanofluid in ducts with double forward-facing steps, J. Taiwan Inst. Chem. Eng. 47 (2015) 28–42.
[2] O. Mahian, et al., Recent advances in using nanofluids in renewable energy systems and the environmental implications of their uptake, Nano Energy (2021) 106069.
[3] R. Sadri, et al., An experimental study on thermal conductivity and viscosity of nanofluids containing carbon nanotubes, Nanoscale Res. Lett. 9 (1) (2014) 1–16.
[4] H. Ghorabaee, et al., The use of nanofluids in thermosyphon heat pipe: a comprehensive review, Powder Technol. (2021).
[5] A.H. Abdelrazek, et al., Thermal performance evaluation for alumina coated MWCNTs composite nanofluid in annular passage of various eccentricities, Powder Technol. 391 (2021) 114–132.
[6] R. Sadri, et al., A facile, bio-based, novel approach for synthesis of covalently functionalized graphene nanoplatelet nano-coolants toward improved thermo-physical and heat transfer properties, J. Colloid Interface Sci. 509 (2018) 140–152.
[7] J.P. Vallejo, et al., Thermophysical, rheological and electrical properties of mono and hybrid TiB2/B4C nanofluids based on a propylene glycol: water mixture, Powder Technol. 395 (2022) 391–399.
[8] M. Bahiraei, M. Naseri, A. Monavari, A second law analysis on flow of a nanofluid in a shell-and-tube heat exchanger equipped with new unilateral ladder type helical baffles, Powder Technol. 394 (2021) 234–249.
[9] A. Aghaei, et al., Effect of horizontal and vertical elliptic baffles inside an enclosure on the mixed convection of a MWCNTs-water nanofluid and its entropy generation, Eur. Phys. J. Plus 133 (11) (2018) 486.
[10] T. Le Ba, et al., Review on the recent progress in the preparation and stability of graphene-based nanofluids, J. Therm. Anal. Calorim. 142 (3) (2020) 1145–1172.
[11] R. Bakhtiari, et al., Preparation of stable TiO2-graphene/water hybrid nanofluids and development of a new correlation for thermal conductivity, Powder Technol. 385 (2021) 466–477.
[12] A.A. Alrashed, et al., The numerical modeling of water/FMWCNT nanofluid flow and heat transfer in a backward-facing contracting channel, Phys. B Condens. Matter 537 (2018) 176–183.
[13] S.A. Bagherzadeh, et al., A novel sensitivity analysis model of EANN for F-MWCNTs–Fe3O4/EG nanofluid thermal conductivity: outputs predicted analytically instead of numerically to more accuracy and less costs, Phys. A 521 (2019) 406–415.
[14] A. Ghasemi, et al., Appraising influence of COOH-MWCNTs on thermal conductivity of antifreeze using curve fitting and neural network, Phys. A 514 (2019) 36–45.
[15] R. Manimaran, et al., Preparation and characterization of copper oxide nanofluid for heat transfer applications, Appl. Nanosci. 4 (2) (2014) 163–167.
[16] M.Z.U. Khan, et al., Investigation of heat transfer in dimple-protrusion micro-channel heat sinks using copper oxide nano-additives, Case Stud. Therm. Eng. 28 (2021) 101374.
[17] S. Soltani, et al., Exergetic and enviromental assessment of a photovoltaic thermal-thermoelectric system using nanofluids: indoor experimental tests, Energy Convers. Manag. 218 (2020) 112907.
[18] M. Hernaiz, et al., The contact angle of nanofluids as thermophysical property, J. Colloid Interface Sci. 547 (2019) 393–406.
[19] H. Goodarzi, et al., Numerical simulation of natural convection heat transfer of nanofluid with cu, MWCNT, and Al2O3 nanoparticles in a cavity with different aspect ratios, J. Therm. Sci. Eng. Appl. 11 (6) (2019).
[20] M.Z.U. Khan, et al., Investigation of heat transfer in wavy and dual wavy micro-channel heat sink using alumina nanoparticles, Case Stud. Therm. Eng. 28 (2021) 101515.
[21] N. Akram, et al., Experimental investigations of the performance of a flat-plate solar collector using carbon and metal oxides based nanofluids, Energy (2021) 120452.
[22] N. Akram, et al., An experimental investigation on the performance of a flat-plate solar collector using eco-friendly treated graphene nanoplatelets–water nanofluids, J. Therm. Anal. Calorim. 138 (1) (2019) 609–621.
[23] A. Feizabadi, M. Khoshvaght-Aliabadi, A.B. Rahimi, Numerical investigation on Al2O3/water nanofluid flow through twisted-serpentine tube with empirical validation, Appl. Therm. Eng. 137 (2018) 296–309.
[24] M. Safaei, et al., Investigation of heat transfer enhancement in a forward-facing contracting channel using FMWCNT nanofluids, Numer. Heat Transf. Part A 66 (12) (2014) 1321–1340.
[25] R. Sadri, et al., CFD modeling of turbulent convection heat transfer of nanofluids containing green functionalized graphene nanoplatelets flowing in a horizontal tube: comparison with experimental data, J. Mol. Liq. 269 (2018) 152–159.
[26] M. Benkhedda, T. Boufendi, S. Touahri, Laminar mixed convective heat transfer enhancement by using Ag-TiO 2-water hybrid nanofluid in a heated horizontal annulus, Heat Mass Transf. 54 (9) (2018) 2799–2814.
[27] H. Jalali, H. Abbassi, Numerical investigation of heat transfer by Al 2 O 3–water nanofluid in square cavity, International Conference Design and Modeling of Mechanical Systems, Springer, 2017.
[28] S. Fotukian, M.N. Esfahany, Experimental study of turbulent convective heat transfer and pressure drop of dilute CuO/water nanofluid inside a circular tube, Int. Commun. Heat Mass Transf. 37 (2) (2010) 214–219.
[29] A. Sajadi, M. Kazemi, Investigation of turbulent convective heat transfer and pressure drop of TiO2/water nanofluid in circular tube, Int. Commun. Heat Mass Transf. 38 (10) (2011) 1474–1478.
[30] M.H. Esfe, S. Saedodin, M. Mahmoodi, Experimental studies on the convective heat transfer performance and thermophysical properties of MgO–water nanofluid under turbulent flow, Exp. Thermal Fluid Sci. 52 (2014) 68–78.
[31] Y. Li, et al., Experimental investigation on heat transfer and pressure drop of ZnO/ethylene glycol-water nanofluids in transition flow, Appl. Therm. Eng. 93 (2016) 537–548.
[32] N.P. Devi, C.S. Rao, K.K. Kumar, Numerical and experimental studies of nanofluid as a coolant flowing through a circular tube, Numerical Heat Transfer and Fluid Flow, Springer 2019, pp. 511–518.
[33] R. Sadri, et al., A bio-based, facile approach for the preparation of covalently functionalized carbon nanotubes aqueous suspensions and their potential as heat transfer fluids, J. Colloid Interface Sci. 504 (2017) 115–123.
[34] E. Gholamalizadeh, et al., Simulation of water/FMWCNT nanofluid forced convection in a microchannel filled with porous material under slip velocity and temperature jump boundary conditions, Int. J. Numer. Method Heat Fluid Flow (2019).
[35] N. Akram, et al., A comprehensive review on nanofluid operated solar flat plate collectors, J. Therm. Anal. Calorim. 139 (2) (2019) 1309–1343.
[36] Y.-P. Sun, et al., Functionalized carbon nanotubes: properties and applications, Acc. Chem. Res. 35 (12) (2002) 1096–1104.
[37] M. Hosseini, et al., Experimental study on heat transfer and thermo-physical properties of covalently functionalized carbon nanotubes nanofluids in an annular heat exchanger: a green and novel synthesis, Energy Fuel 31 (5) (2017) 5635–5644.
[38] C. Golumbic, H. Mattill, The antioxidant properties of gallic acid and allied compounds, Oil Soap 19 (8) (1942) 144–145.
[39] E.J. Weydemeyer, A.J. Sawdon, C.-A. Peng, Controlled cutting and hydroxyl functionalization of carbon nanotubes through autoclaving and sonication in hydrogen peroxide, Chem. Commun. 51 (27) (2015) 5939–5942.
[40] Y. Yang, et al., A facile, green, and tunable method to functionalize carbon nanotubes with water-soluble azo initiators by one-step free radical addition, Appl. Surf. Sci. 256 (10) (2010) 3286–3292.
[41] W. Duangthongsuk, S. Wongwises, Measurement of temperature-dependent thermal conductivity and viscosity of TiO 2-water nanofluids, Exp. Thermal Fluid Sci. 33 (4) (2009) 706–714.
[42] X. Zhang, H. Gu, M. Fujii, Experimental study on the effective thermal conductivity and thermal diffusivity of nanofluids, Int. J. Thermophys. 27 (2) (2006) 569–580.
[43] J. Fernandez-Seara, et al., A general review of the Wilson plot method and its modifications to determine convection coefficients in heat exchange devices, Appl. Therm. Eng. 27 (17) (2007) 2745–2757.
[44] V. Gnielinski, New equations for heat and mass transfer in the turbulent flow in pipes and channels, NASA STI/recon Tech. Rep. A 75 (1975) 22028.
[45] B. Petukhov, Heat transfer and friction in turbulent pipe flow with variable physical properties, Adv. Heat Tran. 6 (1970) 503–564.
[46] W. Duangthongsuk, S. Wongwises, Effect of thermophysical properties models on the predicting of the convective heat transfer coefficient for low concentration nanofluid, Int. Commun. Heat Mass Transf. 35 (10) (2008) 1320–1326.
[47] H. Blasius, Grenzschichten in Flüssigkeiten mit kleiner Reibung, Druck von BG Teubner, 1907.
[48] R.B. Mansour, N. Galanis, C.T. Nguyen, Effect of uncertainties in physical properties on forced convection heat transfer with nanofluids, Appl. Therm. Eng. 27 (1) (2007) 240–249.
[49] W. Ahmed, et al., Characteristics investigation on heat transfer growth of sonochemically synthesized ZnO-DW based nanofluids inside square heat exchanger, J. Therm. Anal. Calorim. 144 (4) (2021) 1517–1534.
[50] W. Thompson, An introduction to error analysis: the study of uncertainties in physical measurements, by John R. Taylor, Phys. Today 51 (1998) 57–58.
[51] M.H. Esfe, et al., Heat transfer characteristics and pressure drop of COOH-functionalized DWCNTs/water nanofluid in turbulent flow at low concentrations, Int. J. Heat Mass Transf. 73 (2014) 186–194.
[52] A.G. Rusu, et al., Thermal behavior of hydrophobically modified hydrogels using TGA/FTIR/MS analysis technique, Thermochim. Acta 613 (2015) 28–40.
[53] A. Ghadimi, I.H. Metselaar, The influence of surfactant and ultrasonic processing on improvement of stability, thermal conductivity and viscosity of titania nanofluid, Exp. Thermal Fluid Sci. 51 (2013) 1–9.
[54] S.J. Aravind, et al., Investigation of structural stability, dispersion, viscosity, and conductive heat transfer properties of functionalized carbon nanotube based nanofluids, J. Phys. Chem. C 115 (34) (2011) 16737–16744.
[55] M. Goodarzi, et al., Experimental evaluation of dynamic viscosity of ZnO–MWCNTs/engine oil hybrid nanolubricant based on changes in temperature and concentration, J. Therm. Anal. Calorim. 136 (2) (2019) 513–525.
[56] M. Goodarzi, et al., Investigation of heat transfer and pressure drop of a counter flow corrugated plate heat exchanger using MWCNT based nanofluids, Int. Commun. Heat Mass Transf. 66 (2015) 172–179.
[57] R. Sadri, et al., Experimental study on thermo-physical and rheological properties of highly stable and green reduced graphene oxide nanofluids: hydrothermal assisted technique, J. Dispers. Sci. Technol. 38 (9) (2017) 1302–1310.
[58] G.H. Ko, et al., An experimental study on the pressure drop of nanofluids containing carbon nanotubes in a horizontal tube, Int. J. Heat Mass Transf. 50 (23) (2007) 4749–4753.
[59] P. Keblinski, et al., Mechanisms of heat flow in suspensions of nano-sized particles (nanofluids), Int. J. Heat Mass Transf. 45 (4) (2002) 855–863.
[60] J.A. Eastman, et al., Thermal transport in nanofluids, Annu. Rev. Mater. Res. 34 (2004) 219–246.

[61] M.L. Ramires, et al., Standard reference data for the thermal conductivity of water, J. Phys. Chem. Ref. Data 24 (3) (1995) 1377–1381.
[62] K. Khanafer, K. Vafai, A critical synthesis of thermophysical characteristics of nanofluids, Int. J. Heat Mass Transf. 54 (19) (2011) 4410–4428.
[63] J.-H. Lee, et al., Effective viscosities and thermal conductivities of aqueous nanofluids containing low volume concentrations of Al 2 O 3 nanoparticles, Int. J. Heat Mass Transf. 51 (11) (2008) 2651–2656.
[64] E.V. Timofeeva, J.L. Routbort, D. Singh, Particle shape effects on thermophysical properties of alumina nanofluids, J. Appl. Phys. 106 (1) (2009) 014304.
[65] W. Yu, et al., Thermophysical property-related comparison criteria for nanofluid heat transfer enhancement in turbulent flow, Appl. Phys. Lett. 96 (21) (2010) 213109.
[66] C. Tsai, et al., Effect of structural character of gold nanoparticles in nanofluid on heat pipe thermal performance, Mater. Lett. 58 (9) (2004) 1461–1465.
[67] J. Qu, H. Wu, Thermal performance comparison of oscillating heat pipes with SiO 2/water and Al 2 O 3/water nanofluids, Int. J. Therm. Sci. 50 (10) (2011) 1954–1962.
[68] S.Z. Heris, M.N. Esfahany, S.G. Etemad, Experimental investigation of convective heat transfer of Al 2 O 3/water nanofluid in circular tube, Int. J. Heat Fluid Flow 28 (2) (2007) 203–210.
[69] H. Yarmand, et al., Experimental investigation of thermo-physical properties, convective heat transfer and pressure drop of functionalized graphene nanoplatelets aqueous nanofluid in a square heated pipe, Energy Convers. Manag. 114 (2016) 38–49.
[70] Y. Ding, et al., Heat transfer of aqueous suspensions of carbon nanotubes (CNT nanofluids), Int. J. Heat Mass Transf. 49 (1) (2006) 240–250.
[71] L.S. Sundar, M.K. Singh, A.C. Sousa, Enhanced heat transfer and friction factor of MWCNT–Fe 3 O 4/water hybrid nanofluids, Int. Commun. Heat Mass Transf. 52 (2014) 73–83.